Small optical volume terahertz emitting microdisk quantum cascade lasers

L. Andrea Dunbar[a] and Romuald Houdré
Institute of Micro- and Optoelectronics, Faculté des sciences de base, Station 3, Ecole Polytechnique Fédérale de Lausanne (EPFL), Lausanne CH-1015, Switzerland

Giacomo Scalari, Lorenzo Sirigu, Marcella Giovannini, and Jérôme Faist
Institute of Physics, University of Neuchâtel, 1 A.-L. Breguet, Neuchâtel CH-2000, Switzerland

(Received 3 January 2007; accepted 4 March 2007; published online 6 April 2007)

The authors fabricate and characterize a series of quantum cascade laser micropillars emitting at ≈3.5 THz. The optical confinement by double plasmon guiding in the vertical direction creates a large impedance mismatch between the confined optical modes and free space. Thus, unlike standard dielectric structures, large quality (Q) factors are maintained for small radius to wavelength ratios. The narrow bandwidth of the optical mode results in low threshold current (8 mA) single-mode lasers. Cavity pulling enables a fine dynamic tuning of the emission wavelength. Comparison of the frequency shift due to cavity pulling and the Stark effect provides an experimental measure of the gain (36 cm^{-1}). © *2007 American Institute of Physics*.
[DOI: 10.1063/1.2719674]

Optical microresonators provide a way to engineer the optical mode spectrum, and as such can control the spectral and spatial light emission for both active and passive devices. This control usually requires both high quality factors (Q) and low modal volumes, these parameters often require conflicting optical resonator properties. In disk dielectric microresonators Q factors with values up to 100 000 000 have been achieved.[1] The achievable Q is ultimately limited by the optical tunneling of these cavities.[2] Thus, very high Q structures retain relatively high $n_{\mathrm{eff}}r/\lambda$ ratios ≈60, where λ is the emission wavelength, n_{eff} is the effective refractive index, and r is the radius.[1]

Injection microdisk semiconductor lasers have been demonstrated at near-infrared wavelengths.[3] Microdisk resonators are also particularly suited to lasers emitting via intersubband transitions as they do not suffer from surface recombination; the first works on microcavity resonators for such devices were using quantum cascade lasers (QCLs) emitting at midinfrared wavelengths.[4,5] More recently microdisks for QCLs emitting at terahertz frequencies using a double metal waveguide for vertical confinement[6] have been investigated; however, the size of the structures remains relatively large with $n_{\mathrm{eff}}r/\lambda \approx 3.5$.

In this work we show that the double plasmon waveguide generated from the metal-metal confinement allows us to fabricate narrow linewidth structures with small modal volumes below the $n_{\mathrm{eff}}r/\lambda = 2$ regime. This is due to the large impedance mismatch of the optical mode between the double plasmon metal waveguide and the surrounding free space. Such a large mode mismatch suppresses the optical tunneling that normally occur in the dielectric structures of equivalent symmetry.

The energy band diagram of the QCL structure studied here is very similar to that described in Ref. 7. The $GaAs/Al_{0.15}Ga_{0.85}As$ active layer is grown by molecular beam epitaxy on a semi-insulating GaAs substrate. To process the devices into a metal-metal waveguide configuration, a Ti/Au layer (5/500 nm) was deposited onto both the QCL structure and a doped GaAs substrate. These were then bonded by means of a thermocompression wafer bonding of the Au/Au surfaces. The original substrate is removed by a mechanical polish followed by a selective wet etch. The pillars are fabricated using standard photolithography to pattern a mask into a photoresist, which is then transferred into a SiO_x hard mask through a CF_4 dry plasma reactive ion etch (RIE). A Cl_2 based chemistry RIE transfers the hard mask into the sample. The epitaxial QCL structure is etched down through the entire active region to the Au layer (≈15 μm), see Fig. 1. The bottom contact is made either through the doped GaAs substrate or by bonding directly onto the area surrounding the pillars. The top contact is formed by depositing a Ti/Au layer. The pillars were then bonded as shown in Fig. 1(b) (inset).

Six different pillar radii were investigated: 20, 27.5, 30, 35, 40, and 50 μm. Electrical and optical characterizations were performed as a function of temperature for the 50 μm pillars which showed laser emission up to 70 K for pulsed operation and 68 K for continuous wave (cw) operation. All other measurements were made at 9 K. All the laser emission measured was single mode, as the optical modes are widely spaced for such low pillar $n_{\mathrm{eff}}r/\lambda$ ratios; with the exception of the 50 μm at high current densities. The structures were characterized by measuring the light current curve, the current voltage curve and spectra were taken using a under vacuum Fourier transform infra-red spectrometer with cryogenically cooled bolometer lock-in detection system with a resolution of 0.03 meV.

Three different pillars of radius of 27.5 μm were tested, similar threshold currents, emission wavelengths, and dynamic ranges of the light current curves were measured. This attests to the reproducibility of the pillar radius to within 2%. Figure 2(a) shows the cw electrical characterization of one of the 27.5 μm radius pillars. The differential resistance (red curve, far left axis) taken from the current voltage measurement shows the characteristic discontinuity at the lasing threshold (8 mA, 337 A cm^{-2}).[8]

The light current curve of several different pillar radii are shown in Fig. 2(b). The light current curve for a ridge

[a]Electronic mail: andrea.dunbar@csem.ch

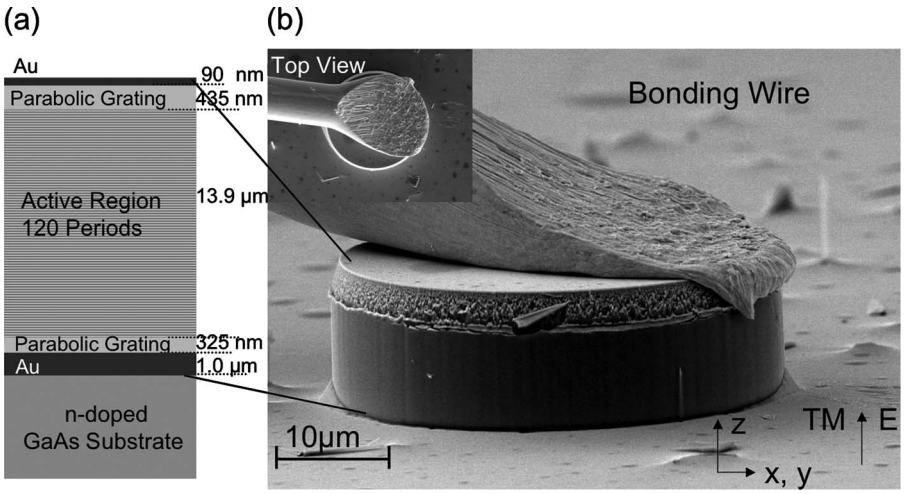

FIG. 1. (a) Schematic of the vertical structure of the pillar. (b) Scanning electron micrscope picture of the bonded 20 μm radius pillar. The structure was etched 15 μm, through the entire active region to the Au layer. Inset left: top view of bonded pillar. Inset right: definition of TM polarization.

waveguide of dimensions of 1.3 mm by 80 μm processed on the same sample with dry etched facets is also shown for comparison. The ridge waveguide rollover begins at $\approx$800 A cm^{-2} as can be seen from its light current curve. The current density range for which lasing is observed for the pillars is reduced compared to that of the ridge waveguide. This reduction is dependent on the interplay of the blue Stark shift of the gain and the optical mode spectrum.

The Stark shift was characterized by measuring the spontaneous emission spectra from an edge emitting[9] mesa as a function of current density (J): $\mathrm{EL}_{\mathrm{peak}}(\mathrm{meV})=2.23\times10^{-3}\ \mathrm{J(A\ cm^{-2})}+13.5$.

Solving for the optical field, $\phi(r,\theta)$, of an ideal cylinder where r is the radial coordinate and θ is the azimuthal angle, with the boundary condition $\phi_{\mathrm{in}}(R,\theta)=0$ gives the solution $\phi_{\mathrm{in}}(r,\theta)=A_M J_M(r n_{\mathrm{eff}} W_{M,N/c})\exp iM\theta$, where J_M are Bessel functions of interger order and A_M is a normalization constant. With the boundary condition imposed the frequencies are given by $\omega_{N,M}=X_M^N c/n_{\mathrm{eff}}R$, where X_N^M is the Nth zero of the $J_M(r)$, M is the number of radial modes and N is the azimuthal number. An n_{eff} of 3.77 is assumed.[10] The low loss optical modes are those of low N; modes with high N correspond to optical modes with internal reflection close to normal incidence. The lowest loss modes are those with $N=1$ and are called whispering gallery modes (WGMs).

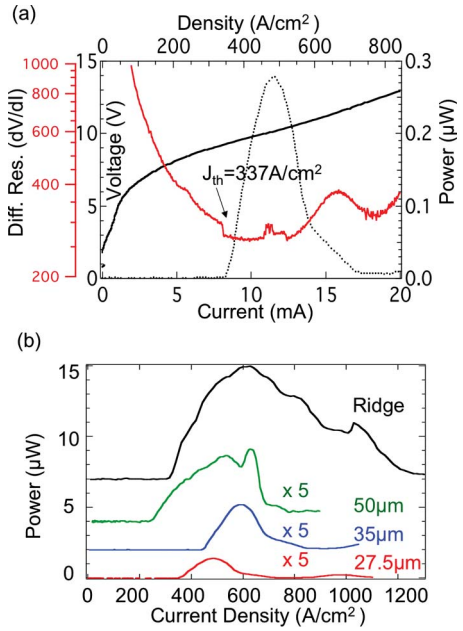

FIG. 2. (Color online) (a) Results under cw operation from a 27.5 μm radius micropillar: differential resistance (red curve and far left axis), voltage (left axis), and light (right axis) all against current density. The lasing threshold is clearly shown at 8 mA. (b) The light current curve for different radii pillars and a ridge waveguide under pulsed operation.

The range of the light current density curve of the pillars is reduced when compared to that of the ridge. When the current increases the total gain increases and blueshifts. Thus with increasing current the gain will sweep across the optical mode. For example, the lasing action of the 27.5 μm radius pillar (red curve) starts at the low current density of $\approx$337 A cm^{-2} but there is a sharp reduction in light emission at a current density of $\approx$600 A cm^{-2} long before the rollover current density. This is caused by the energy mismatch between the peak of the gain and the optical mode. The dynamic range of the lasing depends on the initial energy mismatch between the optical mode energy and the peak energy of the QCL gain, the size of the Stark shift with current density, and the bandwidth of the optical mode.

The dispersion of the WGMs is represented by bold lines in Fig. 3 and all other optical modes are shown with light gray lines. The wavelength range of the x axis is the gain bandwidth. The dashed vertical lines are a guide to the eye for the different radii measured. The calculated E field of the optical mode closest in energy to the lasing energy for a given radius is shown. Figure 3(b) shows the average lasing threshold for the pillar radii measured.

For the micropillars with a radius of 20 μm, no lasing was observed as the gain bandwidth of the QCL does not overlap with an optical mode; the adjacent optical mode energies are at 13.8 meV and 17 meV. The lasing energy of the 40 μm pillar occurs at the energy (1,7) mode, which is a low loss WGM. This low threshold (displayed on the lower part of Fig. 3) is due the fact that the energy of the peak of the gain curve is close to that of the energy of the optical mode at low current densities. Similarly, the 27.5 μm pillar has a low threshold current density as the energy of the QCL gain peak is approximately that of the optical mode at its lasing threshold, i.e., the lasing energy is similar to that of the optical mode. The energies of the lasing emission for the 35 μm radius pillar are 0.29 and 0.44 meV below the (2,3) and (1,6) optical modes, respectively. Although the (1,6) optical mode has intrinsically lower losses its energy difference from that of the lasing energy suggests that lasing occurs at

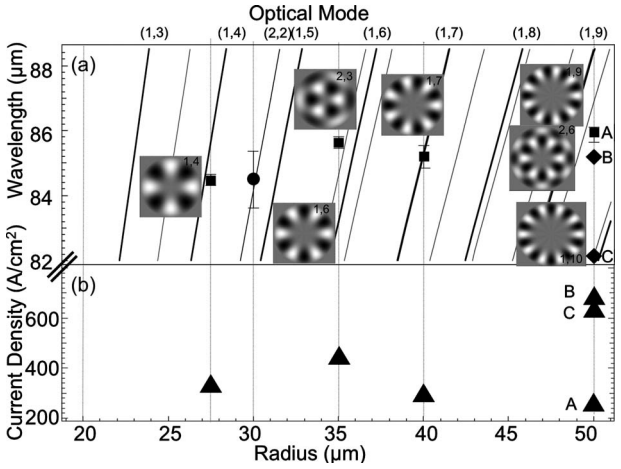

FIG. 3. (a) Black lines represent the allowed optical modes, lines in bold highlight the whispering gallery modes. The dashed vertical lines show the radii of the measured pillar. The emission energy of the lasers is marked by squares. The circular mark shows the peak energy of the EL of the 30 μm radius pillar. The diamonds mark the lasing energies for the 50 μm radius pillar at high current intensities. For the 20 μm radius pillar electrical measurements were made, however, no laser emission was observed. The electric field distribution of the relevant optical modes is shown. (b) The threshold current densities vs diameter.

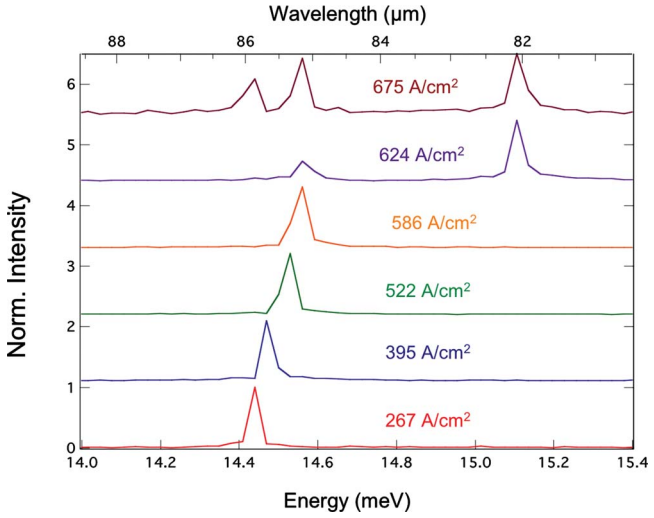

FIG. 4. (Color online) Emission spectra for the 50 μm radius laser for different current densities. The single mode emission shows a steady shift to higher energies with increasing current density. This is due to the diagonal nature of the bound to continuum transition (Ref. 7). At high current densities the lasing emission becomes multimode.

the (2,3) optical mode. The lasing wavelength occurs at precisely the peak of the gain curve at threshold. The high threshold current, 437 A cm^{-2}, is needed to overcome the high losses of the (2,3) optical mode. No lasing action occurs for the 30 μm pillar, this is attributed to the high optical losses of the nearest optical mode (2,2) [which is greater than that of the (2,3) mode] and the reduced size of this pillar which results in a smaller net gain. It is important to note that intense spontaneous emission is observed for the 30 μm pillar at the (2,2) optical mode energy (circle in Fig. 3). This behavior is unlike that of the 20 μm pillar where no optical mode exists at the gain energies. For the 30 μm pillar the current density needed to bring the peak gain into resonance with the (1,5) optical mode is beyond that at which rollover occurs. The energies at which lasing occurs at high densities for the 50 μm pillar are marked by diamonds in Fig. 3; their energy spacing agrees well with that of the optical modes. The large mode spacing corresponding to a change in M from the (1,9) to the (1,10) WGM and the small spacing between the modes require different M and N. The normalized lasing spectrum for current densities is shown in Fig. 4 for the 50 μm pillar. These spectra show that due to "cavity pulling"[11] the laser emission gradually shifts to higher energies with increasing current density. The shift here is $\approx$0.04 meV per 100 A cm^{-2} which corresponds to a shift of 0.01 in the refractive index. The ratio of the Stark shift to that of the frequency pulling gives an estimation of the gain constant. A value of 36 ± 10 cm^{-1} is obtained, from which the Q factor for this active microdisk can be found from the standard formula, $2\pi n_{\text{eff}}/\lambda\alpha_{\text{tot}}$, α_{tot} is the total loss, $Q=81\pm23$. Thus with these microdisks we have a simple method to find the gain constant, and a very precise dynamic tuning of the emission energy which is much sought after for such compact single-mode sources for spectroscopic applications.

[1] D. K. Armani, T. J. Kippenberg, S. M. Spillane, and K. J. Vahala, Nature (London) **421**, 925 (2003).
[2] K. J. Vahala, Nature (London) **424**, 839 (2003).
[3] S. L. McCall, A. F. J. Levi, R. E. Slusher, S. J. Pearton, and R. A. Logan, Appl. Phys. Lett. **60**, 289 (1992).
[4] J. Faist, C. Gmachl, M. Striccoli, C. Sirtori, F. Capasso, D. L. Sivco, and A. Y. Cho, Appl. Phys. Lett. **69**, 2456 (1996).
[5] C. Gmachl, J. Faist, F. Capasso, C. Sirtori, D. L. Sivco, and A. Y. Cho, IEEE J. Quantum Electron. **33**, 1567 (1997).
[6] G. Fasching, A. Benz, K. Unterrainer, R. Zobl, A. M. Andrews, T. Roch, W. Schrenk, and G. Strasser, Appl. Phys. Lett. **87**, 211112 (2005).
[7] G. Scalari, N. Hoyler, M. Giovannini, and J. Faist, Appl. Phys. Lett. **86**, 181101 (2005).
[8] C. Sirtori, F. Capasso, J. Faist, A. L. Hutchinson, D. L. Sivco, and A. Y. Cho, IEEE J. Quantum Electron. **34**, 1722 (1998).
[9] The bottom contact of a single plasmon waveguide adds a surface series resistance: by measuring the injected current density we can compare results obtained from different waveguide configurations and then identify the Stark shift.
[10] L. A. Dunbar, V. Moreau, R. Ferrini, R. Houdré, L. Sirigu, G. Scalari, M. Giovannini, N. Hoyler, and J. Faist, Opt. Express **13**, 8960 (2005).
[11] A. Yariv, *Quantum Electronics*, 4th ed. (Saunders College Publishing, 1991), Chap. 6, p. 181.